Supporting Information for

Activated Transport in Polymer Grafted Nanoparticle Melts

Mayank Jhalaria,[1] Yucheng Huang,[2] Eric Ruzicka,[2] Madhusudan Tyagi,[3,4] Reiner Zorn,[5] Michaela Zamponi,[6] Victoria García-Sakai,[7] Brian C. Benicewicz,[2] Sanat K. Kumar*,[1]

[1]Department of Chemical Engineering, Columbia University, New York, NY, 10027

[2]Department of Chemistry and Biochemistry, University of South Carolina, Columbia, SC, 29208.

[3]NIST Center for Neutron Research, National Institute of Standards and Technology, Gaithersburg, Maryland 20899-6102, United States

[4]Department of Materials Science and Engineering, University of Maryland, College Park, MD 20742, United States

[5] Forschungszentrum Jülich GmbH, Jülich Centre for Neutron Science (JCNS-1) and Institute for Biological Information Processing (IBI-8), 52425 Jülich, Germany

[6]Forschungszentrum Jülich GmbH, Jülich Centre for Neutron Science at MLZ, Lichtenbergstr. 1, 85748 Garching, Germany

[7]ISIS Neutron and Muon Source, Rutherford Appleton Laboratory, Chilton, Oxfordshire, OX11 0QX, UK

Sample Preparation

Poly (methyl acrylate) (PMA) grafted nanoparticles were synthesized by surface initiated reversible addition-fragmentation chain transfer polymerization technique (SI-RAFT). The RAFT agents 4-cyano-4-(((dodecylthio)carbonothioyl)thio)pentanoic acid (Cyano) and 2-(dodecylthiocarbonothioylthio)propanoic acid (DoPAT) was used for the RAFT polymerization. All chemicals were obtained from either Fisher or Acros and used as received unless otherwise specified. Spherical silica nanoparticles (14±4 nm diameter) were obtained from Nissan Chemical. 3-Aminopropyldimethylethoxysilane was purchased from Gelest, Inc. and used as received. Cyano and DoPAT was purchased from Boron Molecular, Inc. Methyl acrylate (MA, 99% Acros) was purified by filtration through an activated basic alumina column. Azobisisobutyronitrile (AIBN) was recrystallized from methanol before use. Molecular weights and dispersity were determined using gel permeation chromatography (GPC) equipped with a Varian 290-LC pump, a Varian 390-LC refractive index detector, and three Styragel columns (HR1, HR3 and HR4, molecular weight range of 100-5000, 500-30000, and 5000-500000 respectively). THF was used as eluent for GPC at 30°C and a flow rate of 1.0 mL/min. GPC was calibrated with poly (methyl methacrylate) (PMMA) standards obtained from Polymer Laboratories.

Cyano/DoPAT (4.9mmol) and 2-mercaptothiazoline (0.58 g, 4.95mmol) were dissolved in 20mL dry CH_2Cl_2. (Dimethylamino)pyridine (DMAP) (61 mg, 0.50 mmol) was added slowly to the solution. After stirring for 30 min at 0ºC, dicyclohexylcarbodiimide (DCC) (1.12 g, 5.45 mmol) was added to the solution and stirred at room temperature for 5 hours. After the reaction, the salt byproduct was removed by filtration. The solvent was evaporated by vacuum and followed by silica gel column chromatography (5:1 mixture of ethyl acetate and hexane) to get activated Cyano/DoPAT as yellow/orange oil.

Silica nanoparticles (20 .0 g, 30 wt% in MEK solution) were added to a round bottom flask with 40 mL THF, 80 µL 3-aminopropyldimethylethoxysilane, and 160 µL methoxy(dimethyl)octylsilane. After purging with N_2 for 30min, the solution was refluxed at 75ºC for 4.5 hours. The solution was then cooled to room temperature and precipitated into hexane. The amine functional silica nanoparticles were recovered by centrifuge at 6000rpm for 5 minutes. The dispersion-precipitation process was repeated two more times. The silica nanoparticles were then

dispersed in 100 mL of THF and activated Cyano/DoPAT was added, the amount depended on the final grafting density required on the silica nanoparticles. The solution was stirred overnight and precipitated into methanol and redispersed in THF. This dispersion-precipitation process was repeated until the supernatant solution was colorless. The nanoparticles were placed in a room temperature vacuum oven to dry.

The functionalized NPs were dispersed in 16mL DMF, and 8.02g methyl acrylate (0.093 mol). AIBN, dissolved in THF (466 μL, 0.01M), was added to the solution, and all were transferred to a dried Schlenk flask. The mixture was degassed by three freeze-pump-thaw cycles, backfilled with nitrogen, and placed in an oil bath at 65°C. The polymerization was quenched in ice water after 12 hours. The solution was poured into methanol to precipitate PMA-grafted nanoparticles. The PMA-grafted nanoparticles were recovered by centrifuging at 5000 rpm for 5 minutes. The precipitated PMA-grafted nanoparticles were dispersed in THF and precipitated in hexanes. The dispersion-precipitation process was repeated for another three times.

To determine the graft molecular weights, the PMA-grafted nanoparticles were cleaved by treating 50mg nanoparticles in 3 mL THF with 60 μL HF (51% aqueous solution) and the supernatant was fed to a GPC to measure the molecular weight of the grafted chain.

Experimental Protocol

Standard cylindrical aluminum cans were used for the experiments on HFBS and IRIS. Supported samples on aluminum substrates were cut to size and loaded into the sample holders, covering the entire surface of the cans. On SPHERES, flat sample holders were oriented at an angle of 45° with respect to the incoming beam to minimize self-shielding of the neutron beam by the sample. Samples were loaded into the holder and lowered into the cryostat – the temperature ramped from room temperature to the lowest measurement temperature (either 358 K or 380 K), apart from the collection of a resolution function where the temperature was first lowered to ≈ 4 K (10 K for IRIS) and a resolution measurement was conducted for ~ 4 hours, and then subsequently slowly ramped to the measurement temperature. Previous TGA measurements have confirmed that there is no sample degradation in the temperature range used for the experiments[7]. Scans were collected in 1 hour blocks for a total of 8 hours (4 hours for IRIS) with an energy range of ±31

μeV for SPHERES, ±15 μeV for HFBS, and ±0.6 meV for IRIS. The measured spectra were first treated with a background subtraction (necessary for SPHERES due to the use of Teflon seals for the sample holder) and normalized to vanadium to account for detector efficiencies. The dynamic structure factors, S(q,ω), were transformed into the time domain through an inverse fourier transform. As the measured $S_{meas}(q,\omega)$ is the actual sample specific dynamic structure factor ($S(q,\omega)$) convoluted with the instrumental resolution R(q,ω), the inverse fourier transform also transform the convolution into simpler multiplicative arithmetic. This enables us to factor out the resolution function in an easier manner to obtain the sample specific intermediate scattering function, I(q,t). Here a_1 and a_2 are the scaling factors to normalize the maximum of S(q,ω) and R(q,ω) to 1.

$$a_1 S_{meas}(q,\omega) = S(q,\omega) \otimes a_2 R(q,\omega)$$
$$I(q,t) = a_1 I_{meas}(q,t)/a_2 R(q,t)$$

The extracted intermediate scattering functions I(q,t) were fitted with stretched exponential functions:

$$I(q,t) = A(q) \times \exp\left(-\left(\frac{t}{\tau_{KWW}(q)}\right)^{\beta}\right) + C$$

The stretching exponent β, the prefactor A(q) ~ 1 and the background term C were held constant across all wavevectors to compute the characteristic relaxation times τ_{KWW}, as our previous work indicated that the stretching parameter β is constant across all wavevectors at T = 420 K[7]. The only other non-fitted parameter in this treatment was C, which could be estimated based on the assumptions of how much scattering would be elastic at infinite times based on the plateau values of the intermediate scattering functions at large q values and larger times. The fits are robust and are not perturbed by small changes in the immobile fraction. Scattering from the core, immobile surface hydroxyl groups and polymer segments tethered to the surface are the most likely contributors to the elastic scattering – and the size of the layer that contributes to the elastic component can be estimated by using the following equation. Here, k_0 is the incoming wavevector and k_1 is the outgoing wavevector. We estimate the thickness of the immobile surface layer to be ~ 1nm.

$$\frac{d^2\sigma}{d\Omega d\omega} = \frac{k_1}{4\pi k_0} N[\sigma_{inc} S_{inc}(q,\omega) + \sigma_{coh} S_{coh}(q,\omega)]$$

To calculate the model free activation energies, all characteristic relaxation times were converted to mean relaxation times using the expression below. This effectively unbiased the effect of the stretching parameter on the relaxation time.

$$< \tau(q) >= \tau_{KWW}(q,T) \frac{\Gamma\left(\frac{1}{\beta(T)}\right)}{\beta(T)}$$

The normalized relaxation times were used for the Arrhenius fits included in the main text, according to the expression

$$< \tau >= \tau_\infty \exp\left(\frac{E_A}{RT}\right)$$

Here τ_∞ is the prefactor and E_A is the parameter of interest i.e. the activation energy. The samples analyzed using this method for the purpose of this manuscript are listed below in Table S1.

Table S1. Materials used for this study. All materials were synthesized using RAFT polymerization

M_n (kDa)	ρ_g(ch/nm^2)	w_{SiO_2}	ϕ_{SiO_2}	Instruments tested on
nPMA		0	0	HFBS, IRIS, SPHERES
29	0.47	0.235	0.15	HFBS
41	0.47	0.193	0.125	IRIS
61	0.47	0.168	0.1	HFBS, IRIS
80	0.47	0.135	0.088	IRIS, SPHERES
88	0.47	0.13	0.085	HFBS, IRIS
100	0.47	0.1	0.07	HFBS, IRIS
136	0.47	0.08	0.05	HFBS, IRIS, SPHERES
64	0.66	0.11	0.066	HFBS, IRIS
82	0.66	0.071	0.042	HFBS, SPHERES
129	0.66	0.044	.026	HFBS, SPHERES
33	0.11	0.48	0.35	IRIS

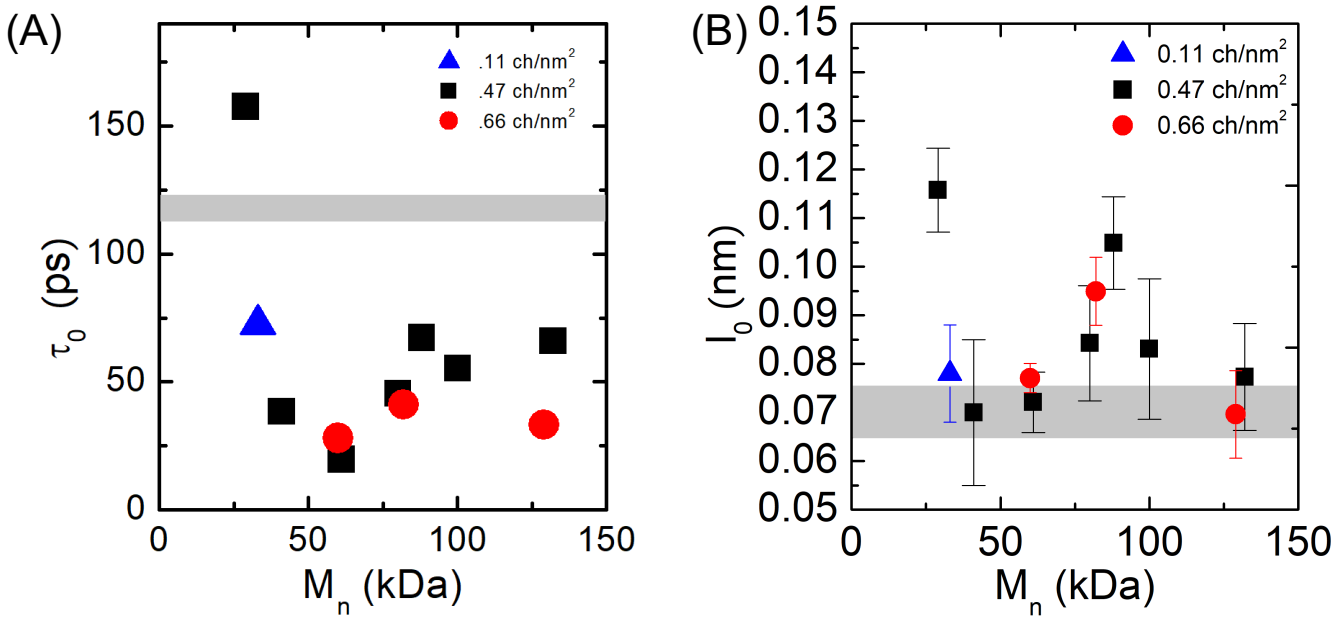

Figure S1. Characteristic jump relaxation times, τ_0 (A) and jump lengths ℓ_0 (B) for all the GNPs included in this study at T = 420 K. The grey band reflects the corresponding values along with error for the neat homopolymer.

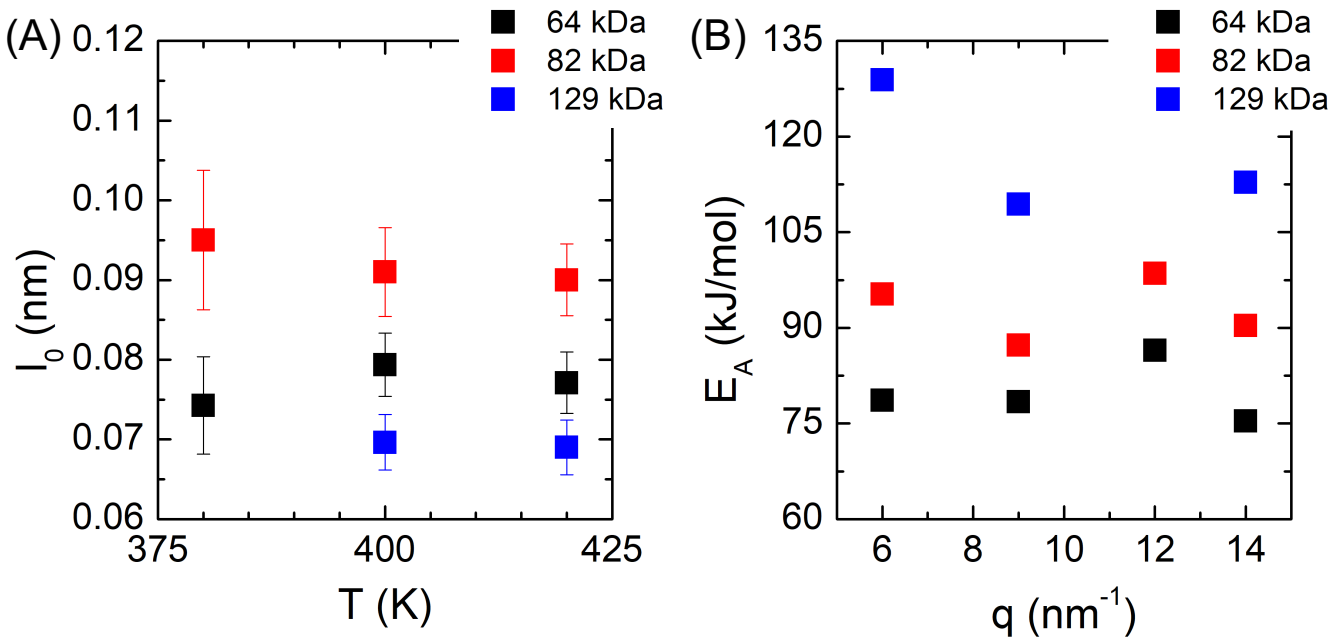

Figure S2. Variation of jump lengths ℓ_0 with temperature (A) and E_A at different wavevectors, q (B) for GNPs with $\rho_g \approx 0.66$ ch/nm^2. Both the jump length and activation energy remain constant with respect to the variable they are plotted against.

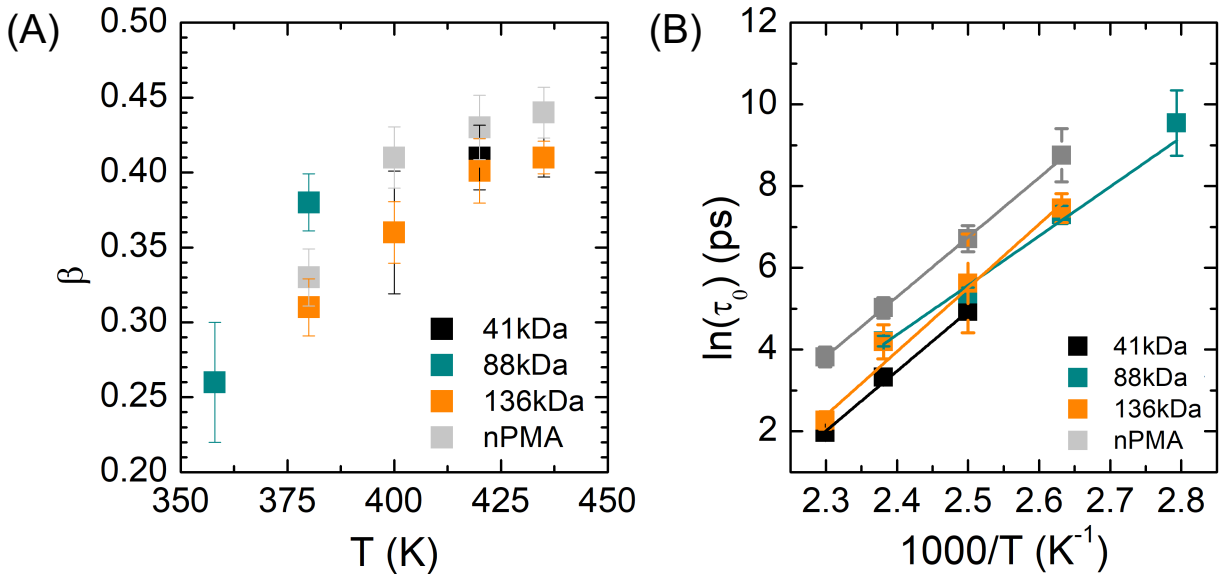

Figure S3. (A) Variation of stretching parameter β with temperature for 3 different GNPs with different M_n – 41, 88 and 136 kDa. The neat homopolymer is shown for reference (grey). (B) Fits to the Arrhenius function (lines) for the same samples shown in part (A). The q value shown here is q = 11.1 nm^{-1}.

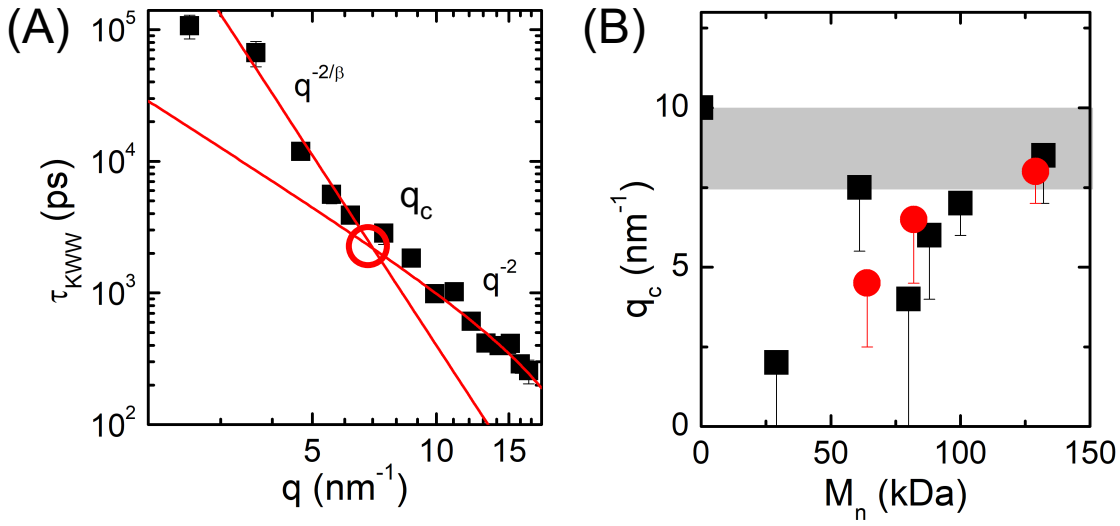

Figure S4. (A) q-dispersion for a PMA homopolymer melt showing the crossover between two asymptotic trends – q^{-2} and $q^{-2/\beta}$ at T = 420 K. The crossover q value q_c is highlighted in the graph. (B) Range of crossover q values for different graft chain lengths and grafting densities (■ – 0.47, ● – 0.66 chains/nm^2). The characteristic crossover length scale ($L \sim 1/q_c$) is larger for the grafted chains as compared to the homopolymer (grey band) in almost all cases.

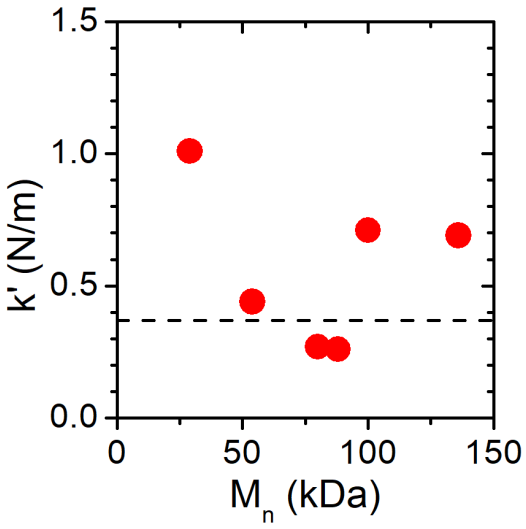

Figure S5. Spring constants (k') calculated from elastic scans for GNPs with $\rho_g \approx 0.47$ ch/nm^2 as well as that of the neat homopolymer (dashed line). Spring constants are calculated from the harmonic approximation to the calculated mean square displacements, $k' = 3k_B/(\frac{d<u^2>}{dT})$. A similar trend to the friction coefficient is observed for the molecular weights studied.

The spring constant shown here is based on a harmonic oscillator assumption for polymers and is based on some early work by Zaccai[1] for proteins. This "spring constant" is not a true representation of the structural spring constant of the polymer chain. Rather it likely relates to the local friction of the medium, as that is what majorly influences the extent of motion of the segments.

Packing model

This model follows from Midya et al.[2] - We assume two spheres in the vicinity of each other such that the polymer brush interact and interpenetrate with each other

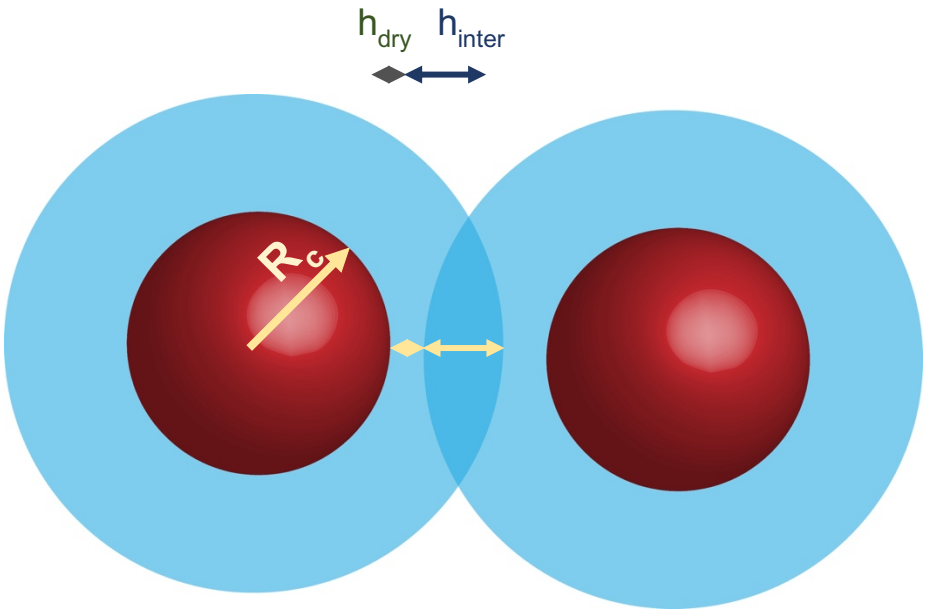

Figure S6. Packing model proposed by Midya et al.[2] where the red core is surrounded by a blue polymer brush. Part of the brush is dry (with length, h_{dry}) and the other part of the brush interpenetrates the brush on a neighboring GNP (h_{inter}). The interpenetrated brush has the conformation of a polymer melt.

For a brush with height and a core size of R_c, space filling conditions from Semenov dictate that

$$\frac{4}{3}\pi(R_c + h)^3 = \frac{4}{3}\pi R_c^3 + \frac{4\pi R_c^2 \rho_g N}{\rho}$$

Here ρ is the monomer density and ρ_g is the grafting density of the chains on the surface of the nanoparticles. Solving this equation gives

$$h = R_c\left[\left(1 + \frac{3\rho_g N}{R_c \rho}\right)^{0.33} - 1\right]$$

The Flory free energy for a chain under extension is defined as the ratio of the dimensions of the chain to the ideal chain dimensions, in this case - $\frac{h}{b\sqrt{N}}$. The chain length at which this quantity is maximized is the maximally stretched chain for this configuration

$$\frac{\partial \ln\left(\frac{h}{b\sqrt{N}}\right)}{\partial N} = -\frac{1}{2N} + \frac{\frac{1}{3}\left(1+\frac{3\rho_g N}{R_c\rho}\right)^{0.33}\frac{3\rho_g}{R_c\rho}}{\left(1+\frac{3\rho_g N}{R_c\rho}\right)^{0.33}-1}$$

Solving this equation gives a universal value for all values of R_c

$$\frac{3\rho_g N_{max}}{R_c\rho} = 19.39$$

N_{max} = 820 (~70 kDa) for R_c = 7 nm, $\rho_g \approx 0.47$ ch/nm^2, ρ = 8.45 monomers/nm^3 which is similar to the observed minimum for the relaxation time and activation energy in the composite systems.

Correlation between packing volume fraction and increased fluctuations

An ansatz that shows the increase of fluctuations with decreasing packing density comes from the work of Zetsche and Fischer [3] and Kant et al.[4] For polymer blends, the volume fluctuations of one component can be calculated from the following equation

$$\delta\phi^2 = \frac{\sqrt{v_A v_B}}{4\pi^2}\int_0^\infty S(q)[qF(q)^2]dq$$

This arises from changes in the self-concentration at small length scales. Using a similar hard sphere mapping described in the main text and the relevant correlation volume defined by the Kuhn length b, the volume fluctuations can be solved for numerically using S(q) derived from the Percus-Yevick[5] closure to the Ornstein-Zernike equation of state. The relevant form factor is defined as

$$F(q) = \frac{[\sin(qb) - qb\cos(qb)]}{(qb)^3}$$

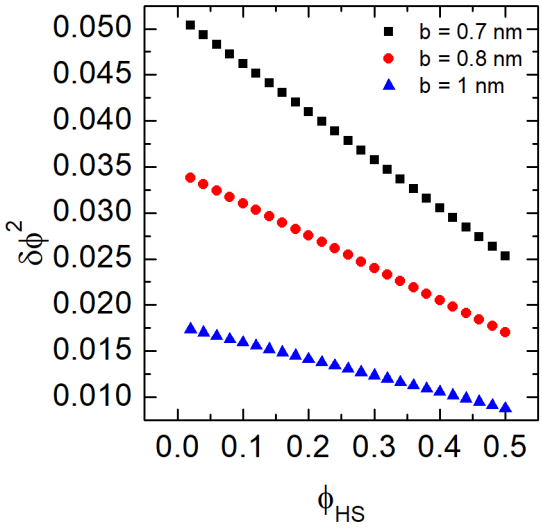

Figure S7. Volume fluctuations for three different Kuhn lengths (hard sphere sizes) at different effective hard sphere volume fractions. With increasing volume fraction the degree of concentration fluctuations decreases

Three volume fluctuation dispersion curves with volume fraction are shown here for three different Kuhn lengths (b = 0.7, 0.8 and 1 nm) i.e. the size of one Kuhn monomer. For the sake of simplicity, we assume that a Kuhn monomers behave as hard spheres with a size defined by the Kuhn Length. As seen from Figure S7, increasing volume fraction of hard spheres (decreasing compressibility)

leads to a continuous drop in the degree of fluctuations in the system, as expected. This is in qualitative agreement with the argument presented in the main text where we posit that increased compressibility of the polymer phase due to inefficient packing leads to the increase in the jump length of segments.

The identification of any commercial product or trade name does not imply endorsement or recommendation by the National Institute of Standards and Technologies.

References

1. Zaccai, G., Biochemistry - How soft is a protein? A protein dynamics force constant measured by neutron scattering. *Science* **2000,** *288* (5471), 1604-1607.
2. Midya, J.; Rubinstein, M.; Kumar, S. K.; Nikoubashman, A., Structure of Polymer-Grafted Nanoparticle Melts. *Acs Nano* **2020**.
3. Zetsche, A.; Fischer, E. W., Dielectric Studies of the Alpha-Relaxation in Miscible Polymer Blends and Its Relation to Concentration Fluctuations. *Acta Polym* **1994,** *45* (3), 168-175.
4. Shenogin, S.; Kant, R.; Colby, R. H.; Kumar, S. K., Dynamics of miscible polymer blends: Predicting the dielectric response. *Macromolecules* **2007,** *40* (16), 5767-5775.
5. Percus, J. K.; Yevick, G. J., Analysis of Classical Statistical Mechanics by Means of Collective Coordinates. *Phys Rev* **1958,** *110* (1), 1-13.